Research Article | Vol. 27, No. 2 | 21 Jan 2019 | OPTICS EXPRESS 804
Optics EXPRESS

Synergy between pyroelectric and photovoltaic effects for optoelectronic nanoparticle manipulation

A. PUERTO,[1] J. F. MUÑOZ-MARTÍN,[2] A. MÉNDEZ,[2] L. ARIZMENDI,[1] A. GARCÍA-CABAÑES,[1] F. AGULLÓ-LÓPEZ,[1] AND M. CARRASCOSA[1,*]

[1]*Departamento de Física de Materiales,Universidad Autónoma de Madrid, calle Francisco Tomás y Valiente 7, 28049 Madrid, Spain*
[2]*Departamento de Mecánica de Fluidos y Propulsión Aeroespacial,Universidad Politécnica de Madrid, Plaza Cardenal Cisneros 3, 28040 Madrid, Spain*
**m.carrascosa@uam.es*

Abstract: The combined action of the pyroelectric (PY) and photovoltaic (PV) effects, exhibited by *z*-cut $LiNbO_3$:Fe substrates, has been investigated for particle trapping and patterning applications. The novel hybrid procedure provides new possibilities and versatility to optoelectronic manipulation on $LiNbO_3$ substrates. It has allowed obtaining periodic and arbitrary 2D patterns whose particle density distribution is correlated with the light intensity profile but can be tuned through ΔT according to the relative strength of the PV and PY effects. A relevant result is that the PY and PV contributions compete for a ΔT range of 1-20 °C, very accessible for experiments. Moreover, the synergy of the PY and PV has provided two additional remarkable applications: i) A method to measure the PV field, key magnitude for photovoltaic optoelectronic tweezers. Using this method, the minimum field needed to obtain a particle pattern has been determined, resulting relatively high, E~60 kV/cm, and so, requiring highly doped crystals when only using the PV effect. ii) An strategy combining the PY and PV to get particle patterning in samples inactive for PV trapping when the PV field value is under that threshold.

1. Introduction

Nano-object manipulation methods constitute nowadays a very active research topic with relevant applications in nanotechnology, photonics and biomedicine [1–3]. Specifically, particle manipulation and trapping methods based on the properties of ferroelectric crystals have been recently proposed and demonstrated. A main technique, the so-called photovoltaic optoelectronic tweezers (PVOT) [4,5], is based on the bulk photovoltaic effect (PVE) exhibited by certain ferroelectrics when suitably doped (notably by Fe doped $LiNbO_3$) [6]. When these crystals are illuminated high electric fields are generated inside the material in accordance with the illumination patterns [7]. The induced fields extend into the surrounding space around the surface of the crystal (evanescent fields) and allow for particle manipulation via electrophoretic (EP) or dielectrophoretic (DEP) forces [5,8] and references therein. The initial experiments were carried out with *x*- or *y*-cut crystals, i.e. with the active surface parallel to the crystal polar axis [9–11]. More recently, nanoparticle (NP) trapping in *z*-cut crystal (polar axis normal to the active surface), with remarkable advantages for 2D patterning, have been reported [12,13]. However, some key parameters of this configuration such as the evanescent electric field, responsible for EP or DEP trapping, are not characterized so far. In particular, the possible existence of a threshold field value for dielectrophoretic trapping is still unclear [12,14]. Nevertheless, this latter configuration of PVOT have found numerous applications in the field of photonics [15], optofluidics [16,17], plasmonics [18] or biotechnology [19]. Another particle manipulation technique based in ferroelectrics uses the pyroelectric effect (PYE) that generates electric fields in pure or doped

#340836 https://doi.org/10.1364/OE.27.000804
Journal © 2019 Received 6 Sep 2018; revised 20 Nov 2018; accepted 30 Nov 2018; published 10 Jan 2019

Optics EXPRESS

$LiNbO_3$ [20,21] associated to the modification of the spontaneous polarization caused by temperature changes [22,23]. Particle patterning using PY fields is less flexible than in the previous case, but it is also possible by domain inversion engineering [20,21] or by using infrared spatially modulated irradiation [24].

Although previous works have considered separately, either the PVE or the PYE, for doped lithium niobate crystals both effects can appear simultaneously, and should, indeed, reinforce or modify the trapping patterns achieved by illumination. It is expected that this interaction present synergetic advantages. On the one hand, it could provide an efficient tool to tailor the particle trapping profiles and offer new possibilities for patterning. On the other hand, in some configurations of photovoltaic tweezers using high light intensities, both effects should appear simultaneously, and substantially affect the formation of the particle trapping patterns. However, no reports on the subject are available so far, except for some promising preliminary results on particle trapping [25]. Moreover, the combination of the two effects has been advantageously exploited for micro-droplet splitting in a recently reported work [26].

The purpose of this work is to investigate the viability of combining the PV and PY effects present in Fe doped $LiNbO_3$ substrates for particle manipulation, characterizing their synergic interaction and potentialities, and determining the main parameters involved. To this end, a pyro-photovoltaic procedure for particle trapping and patterning has been developed first and then, it has been used to obtain a variety of nanoparticle patterns (see sections 4 and 5). The role of different experimental parameters has been studied and the temperature range in which the PV and PY effects compete has been determined. Moreover, sections 6 and 7 present two additional applications of the synergy of the two effects: a method to determine the magnitude of the PV field, taking advantage of its competition with the PY field and a synergic strategy to add PV and PY effects to get trapping patterns in samples developing low PV fields.

2. Physical background

The PV and PY effects in a ferroelectric crystal such as $LiNbO_3$ are, both, a consequence of the polar structure of the crystalline lattice and are reasonably well understood [5,6,22,23]. The PV effect refers to the asymmetric excitation of electrons from certain impurities giving rise to an electric (photovoltaic) current along the polar axis (*c*-axis). Considering a *z*-cut crystal face the PV current density induced along the *c*-axis by a monochromatic illumination of intensity *I* is:

$$j_{PV} = e\alpha\left(\frac{I}{h\nu}\right)l_{PV} \tag{1}$$

where e is the electron charge, α the absorption coefficient, h the Plank constant, ν the light frequency, and l_{PV} the PV drift length. Under open circuit conditions, a charge density σ_{PV} appears at the end z faces, and a bulk PV field, $E_{PV} = \sigma_{PV}/\varepsilon\varepsilon_0$, is generated where ε is the dielectric constant of the crystal. At steady-state conditions, the PV electric field, E_{PV}, and its response time, τ, are given, respectively, by:

$$E_{PV} = \frac{j_{PV}}{e\mu n} = \frac{l_{PV}[\mathrm{Fe}^{3+}]\gamma}{\mu} \tag{2}$$

$$\tau = \frac{\varepsilon\varepsilon_0}{e\mu n} = \frac{\varepsilon\varepsilon_0[\mathrm{Fe}^{3+}]\gamma}{e\mu s I[\mathrm{Fe}^{2+}]} \tag{3}$$

n being the steady density of photo-excited electrons, γ the electron trapping coefficient, s the photoionization cross section, μ the electronic mobility, and $[Fe^{3+}]$ and $[Fe^{2+}]$ the

Optics EXPRESS

concentration of Fe^{+3} and Fe^{+2} respectively (obviously $[Fe^{2+}] + [Fe^{3+}] = [Fe]$). More details can be found in references [4,5].

On the other side, the PY response is related to the surface charge associated to the spontaneous polarization $\mathbf{P}_s$, $\sigma = \mathbf{n}\cdot\mathbf{P}_s$, (where $\mathbf{n}$ is the unity vector normal to the crystal surface), which is usually compensated by external charges. After a sudden change ΔT in the sample temperature, the polarization undergoes a corresponding change and induces a uniform uncompensated surface charge. The difference in charge density ($\Delta\sigma$) creates an evanescent field that could trap nanoparticles. The expression for that pyroelectric charge density, $\sigma_{PY} = \Delta\sigma$, is given by:

$$\sigma_{PY} = \Delta\sigma = \mathbf{n}\cdot\Delta\mathbf{P}_S = c_p \Delta T \tag{4}$$

$c_p = -4 \times 10^{-9}$ $CK^{-1}cm^{-2}$ being the pyroelectric coefficient near room temperature, reported by Savage [27].

In this work, we combine the two effects (PVE and PYE) to generate trapping patterns of nanoparticles. For the analysis of our experiments an additive superposition of the two effects, will be assumed and so, the surface charge density σ_T and electric field is, just, the sum of those corresponding to each particular effect (coupling effects are ignored). This model is schematically represented in Fig. 1 for a negative [Fig. 1(a)] and a positive [Fig. 1(b)] crystal temperature variation and considering the $+z$ crystal surface (see the inset in Fig. 1). This additive approximation to the problem is well adapted to the experimental procedure used in this paper (see section 3). However, in other possible experimental cases when light induces heating and so, PYE simultaneously to PVE, more complex models involving coupling between the two effects would be probably required, but this analysis is beyond the scope of this work.

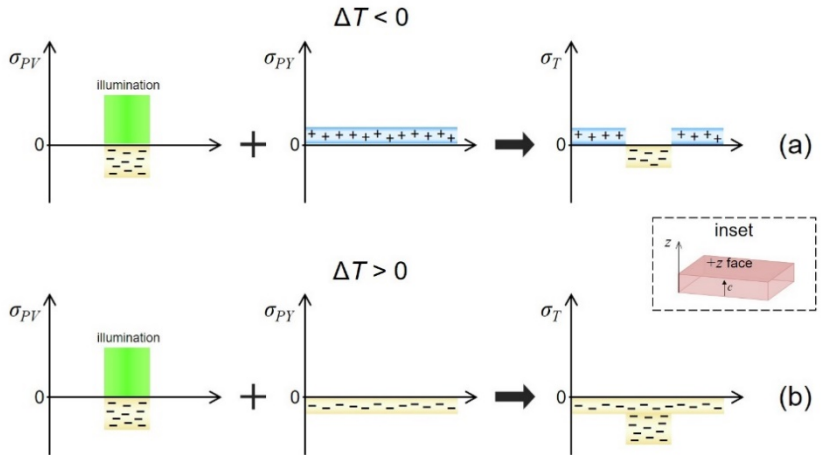

Fig. 1. Schematics of the surface charge induced in the substrate $+z$ face (see inset) by the PVE (left), PYE (center) and both of them (right) for (a) ΔT<0 °C, and (b) ΔT>0 °C.

Anyhow, for particle trapping applications the relevant point is the extension of those fields along the outside space close to the sample surface. The value of these edge fields, called evanescent fields along this work, is governed by the electromagnetic boundary conditions, as described in [5]. The trapping action of the overall field on neutral (non-charged) particles is determined by the associated dielectrophoretic forces [5,8],

$$\mathbf{f}_{DEP} = -\nabla\left(-\mathbf{p}\cdot\mathbf{E}\right) \tag{5}$$

$\mathbf{p}$ being the dipolar momentum of the particle induced by the evanescent electric field $\mathbf{E} = \mathbf{E}_{PY} + \mathbf{E}_{PY}$, assuming additivity of the two fields.

Optics EXPRESS

3. Experimental methods

To perform the experiments three *z*-cut $LiNbO_3$:Fe crystals, purchased from Hangzhou Freqcontrol Electronic Technology Ltd., with two different doping levels have been used, as specified in Table 1. There, it is also indicated the Fe^{2+} concentration, $[Fe^{2+}]$, obtained from the measured absorption coefficient α as $[Fe^{2+}] = \alpha/s$, where $s = 4.55 \times 10^{-18}$ cm^2 is the photoionization cross section, reported by Kurz et *al*. [28] for the absorption band of Fe^{2+} in $LiNbO_3$. The particles used are silver spherical nanoparticles, with an average diameter of 100 nm, bought to Skyspring Nanomaterials Inc..

Table 1. Parameters related to the iron impurity for $LiNbO_3$ substrates used in the experiments.

sample	[Fe] cm^{-3}	$[Fe^{2+}]$ cm^{-3}	$[Fe^{3+}]$ cm^{-3}
1	4.25×10^{19}	4.7×10^{18}	3.8×10^{19}
2	4.25×10^{19}	7.2×10^{18}	3.5×10^{19}
3	1.2×10^{19}	2.9×10^{18}	9.0×10^{18}

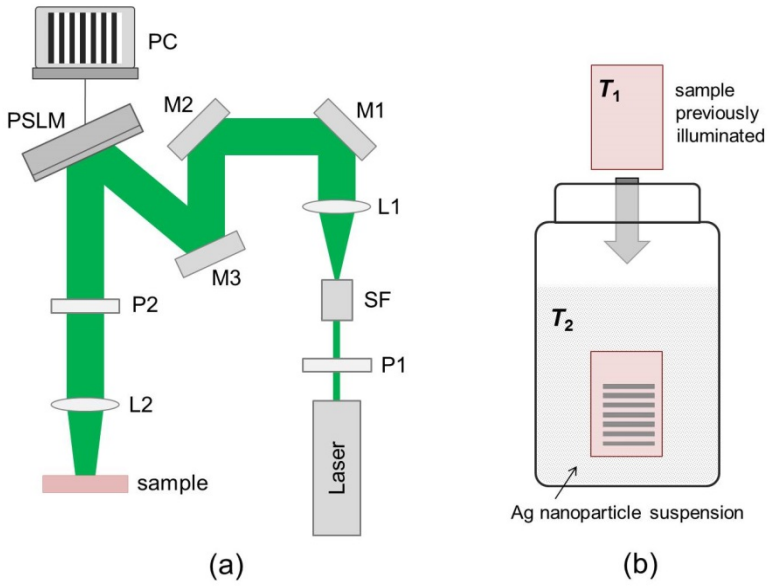

Fig. 2. (a) Optical setup used to illuminate the sample (first step): P1 and P2 are linear polarizers; SF is a spatial filter; L1 and L2 are lenses; M1, M2 and M3 are plane mirrors, and PSLM is a reflection phase spatial light modulator. (b) In the second step the sample, at a temperature T_1, is immersed in the suspension of the Ag nanoparticle kept at a temperature T_2 during 30 seconds in absence of any illumination.

A typical procedure for PV nanoparticle patterning on the active substrate includes two steps. First, the crystal sample is illuminated at a temperature T_1 with a certain light pattern to induce PV electric fields [see Fig. 2(a)]. Next, in the absence of illumination, the crystal is immersed during about 30 s in a non-polar liquid suspension of the particles kept at a temperature T_2 [Fig. 2(b)]. In this second step, the particles deposit under the action of the total dielectrophoretic forces. Thus, the crystal temperature experiences a change $\Delta T = T_2 - T_1$ during immersion and so, a PY field is induced, in addition to the previously established by illumination (first step). For comparison, in some case, we will use only PV trapping by keeping the particle suspension at the same temperature T_1 as during the first stage.

The crystal is illuminated by light profiles provided by a spatial light modulator (HOLOEYE, LC-R1080). Light comes from a frequency doubled Nd:YAG laser operating at 532 nm, with typical intensities in the range 1-10 mW/cm^2. The particle suspension is

Optics EXPRESS

obtained by introducing 0.05 g/l of the Ag nanoparticles in heptane and then sonicated to assure an homogeneous distribution of particles. Finally, the crystal and suspension temperatures are measured by an infrared digital thermometer (Lutron, model TM-939).

4. PV and PY effects competition for particle patterning

The designed strategy consists in combining the PV and PY effects to find a final field profile that might provide an advantageous configuration for particle trapping and patterning. As stated above, during illumination a patterned PV electric field is produced. In the second step, a spatially homogeneous PY field is induced by cooling the sample inside the particle suspension. During this second stage, the suspended particles undergo the electric PV + PY fields and deposit on the sample surface. When the suspension is at lower temperature, the PV and PY surface charges have opposite sign, giving rise to a competition between both effects. To illustrate this competition and to investigate the ability of the pyro-photovoltaic method to obtain particle patterns we have developed a series of experiments using sample 1 with the same illumination fringe pattern, similar to the one that appears in the scheme of Fig. 2(a). The fringe period was Λ = 300 μm, the average light intensity 1.6 mW/cm^2 and the illumination time 10 minutes. The initial temperature T_1 of the sample just before immersion ranges between 22 and 28°C. The temperature decrease of the nanoparticle suspension with regard to the sample was in the range 0 to 20 °C. Hence, the illumination, and therefore the PV effect, is constant in all the set of experiments in this section but the PY contribution is changing. The results are shown in Fig. 3, where photographs of the obtained nanoparticle patterns are shown for ΔT = 0 °C (for reference with only PVE), –5 °C, –8 °C, –10 °C, –15 °C and –20 °C [Figs. 3(a)-3(f), respectively]. The results of the experiment can be more quantitatively appreciated by the corresponding average particle density profiles, obtained from the images, that appear on the right of each figure.

In Fig. 3(a), with ΔT = 0 °C, it is observed the typical PV-induced nanoparticle pattern for *z*-cut, i.e. a replica of the light pattern [13]. In Fig. 3(b), with ΔT = –5 °C, we can see a pattern presenting a double periodicity, i.e. additional particle fringes that arise in the middle of the dark regions of the light pattern. This can be even better observed in the corresponding particle density profile. The relative density of the PV fringes diminishes for ΔT = –8 °C [Fig. 3(c)] and disappears in Fig. 3(d), with ΔT = –10 °C, where the PY effect is high enough to fully compensate the PV-induced charge and so, particles deposit only in the dark regions. For the last two photographs associated to ΔT = –15 °C and –20 °C, respectively, a background of particles adds to the patterned component reducing the visibility of the structure. In Fig. 3(e) the fringes are still visible but become undistinguishable in Fig. 3(f).

The results can be explained qualitatively by the proposed additive model for ΔT<0 schematically represented in Fig. 1(a). In the first step, the light induces a negative surface charge density (only PV-induced) in the illuminated regions producing particle trapping. This is the case of the pattern of Fig. 3(a), taken as reference. Second, the PY effect adds a continue background of positive surface charge density whose level is linear with ΔT. The particles undergo DEP forces associated to the electric field generated by the total net charge. Two situations can be distinguished for the patterns of Fig. (3): i) When $|\sigma_{PY}|<|\sigma_{PV}|$ [Figs. 3(b) and 3(c)], there are alternating positive and negative surface charge regions. Then, a new fringe appears between the PV fringes because DEP forces are independent of the sign of the charge that generates the field, and particles are attracted to fringes with positive PY and negative PV charge density. ii) When $|\sigma_{PY}|>|\sigma_{PV}|$, and consequently the σ_T is always positive. Then, only fringes in non-illuminated regions appear over a background of particles [Figs. 3(e) and 3(f)]. Finally, Fig. 3(d) shows the transition between the two cases that is characterized for an exact compensation between surface charges of the two signs: $|\sigma_{PY}| = |\sigma_{PV}|$ in the illuminated zones. Hence, the corresponding PV and PY fields are also equal. In this case, a "negative" of the light pattern is obtained, i.e., particle trapping only occurs in the dark regions. This case will play a key role in the novel method proposed in section 6 to measure

Optics EXPRESS

the photovoltaic field in *z*-cut samples. Moreover, from the results, we have determined the experimental range of ΔT (5-20 °C), very accessible in practice, in which the two effects compete effectively in the sample.

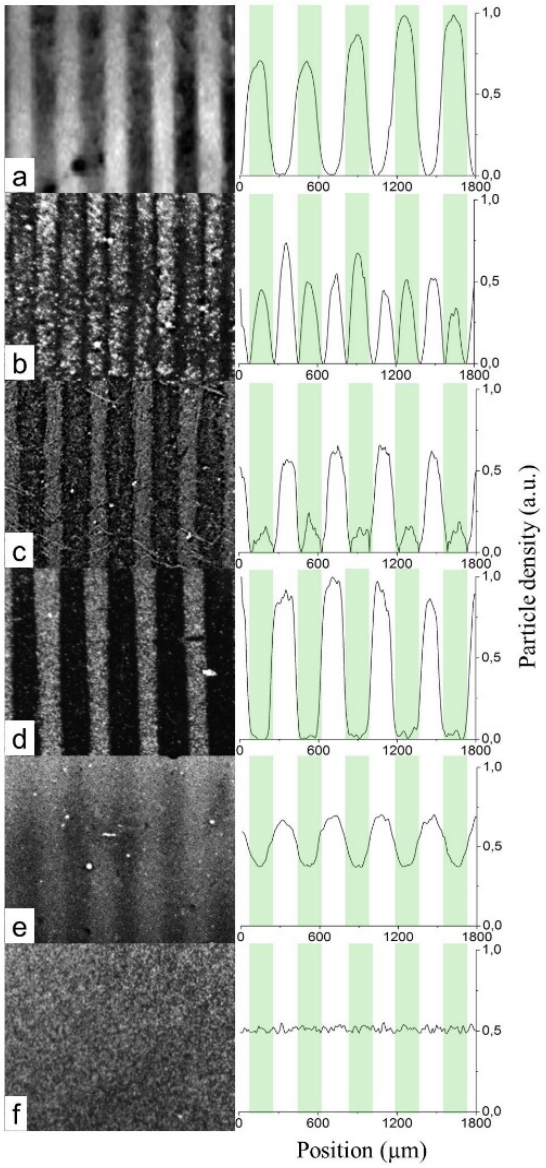

Fig. 3. Photographs of Ag NP patterns deposited on the + *c* sample surface after illumination with a fringe light pattern (green fringes on the right side of the figure) at different temperature change: (a) $\Delta T = 0$ °C, (b) $\Delta T = -5$ °C, (c) $\Delta T = -8$ °C (d) $\Delta T = -10$ °C, (e) $\Delta T = -15$ °C, (f) $\Delta T = -20$ °C. The exposition time is 10 minutes and the light pattern intensity is 1.6 mW/cm^2. On the right of each figure, the corresponding particle density profiles are shown (see text). The fringes have a spatial periodicity of 300 μm.

5. Arbitrary 2D patterns

In order to confirm the previous results and to further visualize the combined effect of the PY and PV contributions, the method has been applied keeping the same experimental parameters, light intensity, exposition time, particle suspension and $\Delta T = -10$ °C, but

Optics EXPRESS

illuminating with a more complex light pattern, consisting in an arbitrary 2D image. For reference, a particle pattern using only the PVE is also shown in Fig. 4(a) whereas Fig. 4(b) shows the corresponding patterns using the combination of PV and PY effects.

The pyro-photovoltaic pattern for $\Delta T = -10$ °C shown in Fig. 4(b) is again a "negative" version of the PV pattern [Fig. 4(a)]. In other words, as it can be expected from the simple model explained above, a "negative" pattern is also obtained for $\Delta T = -10$ °C regardless the shape of the light pattern used as far as the exposition time, light intensity and ΔT are unaltered.

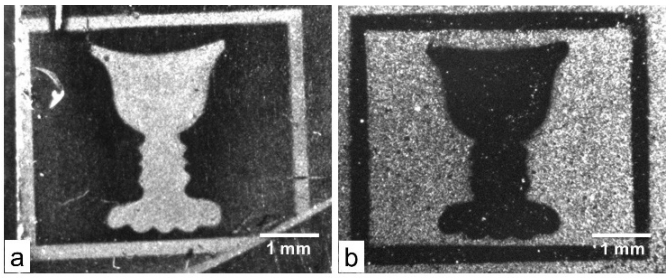

Fig. 4. Photographs of Ag NP patterns deposited on the + z surface with an arbitrary light pattern at (a) $\Delta T = 0$ °C, (b) $\Delta T = -10$ °C (corresponding to a negative pattern). The exposition time was 10 minutes and the light pattern intensity was 1.6 mW/cm^2.

In the next sections, we will report additional applications for the synergy of the PVE and PYE based in the particle patterning experiments.

6. Measurement method of the PV evanescent field

The results on the competition of the PY and PV effects, has allowed designing a convenient experimental method to determine the value of the PV evanescent electric field acting on particles. This is a key operation parameter for photovoltaic tweezers for particle trapping on z-cut crystals not well characterized so far.

The method to determine this electric field is directly based on the generation of a negative particle pattern with regard to the purely photovoltaic pattern. For this negative pattern the PV-induced surface charge density in the illuminated regions compensates exactly the pyroelectric surface charge density: $|\sigma_{PV}| = |\sigma_{PY}| = c_p \Delta T$. Note that internal compensation of PY charge by dark conductivity [29] can be neglected because the corresponding time constant [30] is around 10^3 s, much greater than the times involved in our experiments. Using simple electrostatic relations, the evanescent photovoltaic field at distances much smaller than the size of the illuminated areas can be obtained as:

$$E_{PV} = \frac{|\sigma_{PV}|}{2\varepsilon\varepsilon_0} = \frac{|\sigma_{PY}|}{2\varepsilon\varepsilon_0} = \frac{c_p \Delta T}{2\varepsilon\varepsilon_0} \tag{6}$$

where ε is the static dielectric constant of the heptane ($\varepsilon = \varepsilon_{hep} = 1.9$) [31]. Therefore, the key point of the method is to determine the temperature variation ΔT for which a negative pattern of the PV pattern is obtained. Using the value already mentioned for the pyroelectric coefficient reported by Savage (-4×10^{-9} CK^{-1}cm^{-2}) [27] and $\Delta T = -10$ °C (that generates a negative pattern in sample 1 with exposure time $t = 10$ min), a photovoltaic field value $E_{PV} = 1.2 \times 10^5$ V/cm.

Moreover, keeping a constant intensity it is possible to measure the time kinetics for the generation of the PV electric field by determining, for each exposure time t, the ΔT needed to obtain the negative pattern, i.e., to reach a PY evanescent field that equals in absolute value the E_{PV} field. The results for sample 2 are shown in Fig. 5. Here, for each recording time the

Optics EXPRESS

temperature difference to obtain a negative pattern (right axis), and the corresponding E_{PV} value outside but very close to the sample surface (left axis) are plotted. The inset illustrates one example of a "negative pattern" corresponding to the E_{PV} value indicated in the figure. Note that for the same exposure time, t = 10 min, the obtained value for E_{PV} for this sample is similar to the one previously obtained for sample 1.

The solid line is a single exponential fit to the experimental points given by:

$$E_{PV} = E^{sat}\left(1 - e^{-t/\tau}\right) \tag{7}$$

From the fitting a saturation electric field E^{sat} = (2.5 ± 0.1) × 10^5 V/cm, and a time constant of τ = 11 ± 1 min, are obtained. The temperature difference corresponding to this E^{sat} field, i.e. the one that provides $|\sigma_{PV}| = |\sigma_{PY}|$, is ΔT = –21 ± 0.5 °C.

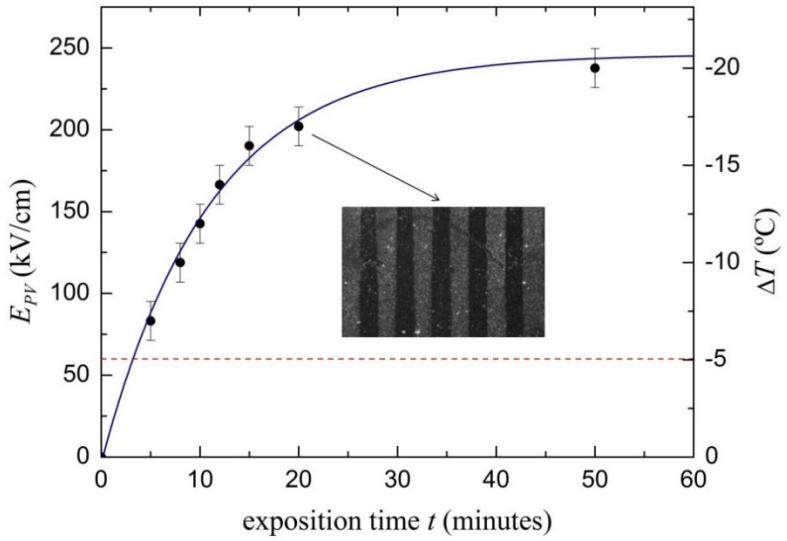

Fig. 5. Temperature difference (right axis) to obtain a negative pattern and (left axis) edge PV field closed to the crystal as a function of the light exposure time (see text). The light intensity used in the experiments is 1.6 mW/cm^2. The inset image is a representative negative pattern corresponding to the indicated point. The solid line is an exponential fit to the data and the dashed red line represent the threshold value.

It worthwhile remarking that, for a rather small temperature difference (in the range of 5-21 °C), the pyroelectric effect compensates the bulk photovoltaic effect indicating an effective competition of both phenomena. Moreover, the saturating PV fields are really large, about 250 KV/cm, assuring a very effective particle trapping. Note that evanescent fields are in this case even larger than bulk fields in a factor $\varepsilon_{LN}/\varepsilon_{hep}$ = 15, where ε_{LN} and ε_{hep} are the dielectric constant of lithium niobate and heptane, respectively.

Finally, it has not been possible to obtain PV particle patterns for time exposures lower than 3 minutes corresponding to $E_{PV} \leq 6 \times 10^4$ V/cm. This suggests that this PV field value is a threshold field, E^{th}, for z-cut particle patterning by DEP forces. Since the PV field inside the crystal, and so, the evanescent PV field is proportional to [Fe^{3+}] [see Eq. (2)] the field threshold implies a corresponding threshold for [Fe^{3+}] and roughly, for the iron doping concentration that is usually, only slightly higher (see values in Table 1). Taking into account the $E^{sat}/E^{th} \approx 4$ and the Fe concentration of this sample, one obtains a threshold concentration $[Fe]^{th} \approx 10^{19}$ cm^{-3}. Note, that this threshold probably has some dependence on the kind of particle though its electronic polarizability.

Optics EXPRESS

Table 2. Impurity concentration and PV parameters of sample 3.

[Fe] cm^{-3}	[Fe^{2+}] cm^{-3}	[Fe^{3+}] cm^{-3}	E^{sat} V/cm	τ* s
1.2×10^{19}	2.9×10^{18}	9.0×10^{18}	5.4×10^{4}	376

*For I = 1.6 mW/cm^2.

To further investigate this important point, we have carried out a patterning experiment in sample 3, whose iron doping is close to the threshold concentration (see Table 2). The illumination fringe pattern and light intensity is the same as in Fig. 3 (Λ = 300 μm, I = 1.6 mW/cm^2). The time exposure was 15 min to reach the saturation field E^{sat}. As it can be seen in Fig. 6(a), no particle pattern can be distinguished in the photograph, although the particle density average profile shows an incipient particle structuration. Therefore, the obtained result, using a different sample with a doping level roughly coinciding with the iron concentration threshold, is a further confirmation of the existence of a threshold value in the PV field and in the iron concentration for DEP trapping and patterning in *z*-cut samples.

7. Pyroelectric activation of substrates with insufficient iron doping

The results of the previous section indicate that photovoltaic tweezers, operating with *z*-cut substrates, require high iron doping, unusual for available commercial $LiNbO_3$:Fe crystals. In this section, we have investigated the viability of adding the PY and PV effects to achieve particle patterning for samples under the threshold Fe concentration. To this end, we have experimented with sample 3, with a concentration just below the threshold for which no patterning was obtained with only PVE [see Fig. 6(a)]. The pyro-photovoltaic experimental method has been applied by heating the sample (instead of cooling) in the particle suspension. This way, a PY-induced spatially constant surface charge density of the same sign is added to the PV-surface charge density enhancing the total electric field. Successful results have been obtained using the same light pattern as in previous Fig. 6(a), but now applying temperature changes as low as ΔT = + 1 °C or + 2 °C. Note that according to Fig. 5 a temperature variation of one degree generates an E_{PY} of about 12 kV/cm. In Fig. 6(b), a representative result with ΔT = + 1 °C is shown. Either in the photograph and in the particle density profile a particle pattern is now clearly visible.

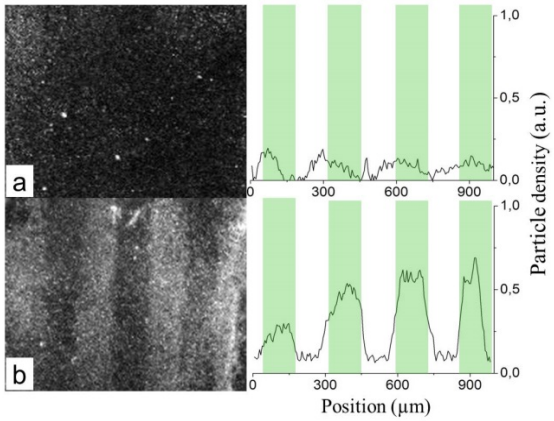

Fig. 6. Photographs of Ag NP patterns deposited on the + *c* surface of sample 3 using a fringe light pattern (green fringes) at different temperature changes: (a) ΔT = 0 °C, (b) ΔT = + 1 °C. The exposition time is 15 minutes and the light pattern intensity is 1.6 mW/cm^2. On the right of each figure, the corresponding particle density profiles are shown (see text). The fringes have a periodicity of 300 μm.

8. Discussion and conclusions

The results of this work demonstrate, for the first time to our knowledge, the viability of combining the PVE and PYE present in $LiNbO_3$:Fe for optoelectronic particle manipulation.

Optics EXPRESS

The proposed experimental method is a slight modification of a procedure commonly used with PV optoelectronic tweezers [5,32]. In this sense, the additional activation of the PYE extends the possibilities and versatility of that powerful technique with a little experimental change.

$LiNbO_3$:Fe has resulted an excellent material for this combination, due to the high value of both effects, PVE and PYE, around room temperature. In fact, one relevant outcome of the work is the range of ΔT with efficient competition of both effects (1-25 °C) that is very accessible for experiments. We have found different particle trapping possibilities by tuning the temperature change ΔT: from a positive pattern to its negative version, passing, for intermediate ΔT, through particle structures with a double spatial frequency. The results obtained are reasonably consistent with an additive behavior for the PV and PY effects. It is worthwhile remarking that the hybrid technique presents a main physical difference with regard the purely PV method. In the latter case, only charge of a sign is generated in each sample surface whereas in the hybrid case, there are regions with charge of the two signs that can be tailor through the light exposure time and the temperature variation.

Moreover, the pyro-photovoltaic technique provides very relevant information for the PV tweezers in *z*-cut. The detailed analysis of PV + PY trapping results has suggested a simple method for the determination of the photovoltaic evanescent electric field value. This measurement was a difficult task when using standard optical or electrical techniques. In fact, only a very recent paper has attempted another indirect, and apparently more complicated strategy, to measure PV fields in *z*-cut samples, based in the orientation of liquid crystals [33].

It is worthwhile noting that our method needs to know the value of the pyroelectric coefficient [see Eq. (6)]. In this work, the value reported by Savage [27], which is a classical reference for lithium niobate has been used. However, to assure highly accurate values for the PV fields, it would be appropriate to directly measure the pyroelectric coefficient in the same sample used for the PV experiments.

Our method has allowed to obtain the kinetics of the generation of the PV evanescent field and, in particular, to measure the saturation E_{PV} value that, for strongly doped crystals, could reach values as high as 2.5×10^5 V/cm. A second consequence of these measurements has been to determine a minimum E_{PV} value for effective particle manipulation, that in our experimental conditions is 6×10^4 V/cm. This E_{PV} threshold implies, in turn, that strongly iron doped crystals ($[Fe]^{th} \geq 10^{19}$ cm^{-3}) are required for PV tweezer operation. This fact is probably the reason why other authors reported [12,14] that DEP trapping in *z*-cut crystals is not possible. The last remark inferred from these results is that, due to the large PY fields generated by small temperature changes of 1-2 °C, when operating with PV tweezers, the control of the substrate and particle suspension temperatures should be very critical to avoid undesired PY contributions.

Finally, if the PV electric field is below but near to the threshold, the photo-pyroelectric method could be still used for effective trapping. The combination of both effects allows to trap and structure nanoparticles according to the illumination pattern.

In summary, the proposed photo-pyroelectric method has demonstrated efficient particle manipulation, showing that a variety of interesting modifications of the trapping patterns can be achieved, that may offer novel and versatile possibilities for trapping and patterning. Additionally, the combination of both effects allows the determination of relevant parameters for the control and optimization of photovoltaic optoelectronic tweezers and other applications of the photovoltaic effect such as liquid crystal orientation [34,35] or all-optical control of graphene charge transport [36].

Funding

Ministerio de Ciencia, Innovación y Universidades of Spain (MAT2014-57704-C3, MAT2017-83951-R); Universidad Politécnica de Madrid (RR01/2016).

Optics EXPRESS

References

1. D. G. Grier, "A revolution in optical manipulation," Nature **424**(6950), 810–816 (2003).
2. P. Y. Chiou, A. T. Ohta, and M. C. Wu, "Massively parallel manipulation of single cells and microparticles using optical images," Nature **436**(7049), 370–372 (2005).
3. A. García-Cabañes, A. Blázquez-Castro, L. Arizmendi, F. Agulló-López, and M. Carrascosa, "Recent achievements on photovoltaic optoelectronic tweezers based on lithium niobate," Crystals **8**(2), 65 (2018).
4. J. Villarroel, H. Burgos, A. García-Cabañes, M. Carrascosa, A. Blázquez-Castro, and F. Agulló-López, "Photovoltaic versus optical tweezers," Opt. Express **19**(24), 24320–24330 (2011).
5. M. Carrascosa, A. García-Cabañes, M. Jubera, J. B. Ramiro, and F. Agulló-López, "$LiNbO_3$: A photovoltaic substrate for massive parallel manipulation and patterning of nano-objects," Appl. Phys. Rev. **2**(4), 040605 (2015).
6. B. Sturmann and V. Fridkin, *Photovoltaic and photorefractive effects in noncentosymetric materials* (Gordon and Breach Science publishers, 1992).
7. E. M. De Miguel, J. Limeres, M. Carrascosa, and L. Arizmendi, "Study of developing thermal fixed holograms in lithium niobate," J. Opt. Soc. Am. B **17**(7), 1140–1146 (2000).
8. T. B. Jones, *Electromechanics of particles* (Cambridge University, 1995).
9. H. A. Eggert, F. Y. Kuhnert, K. Buse, J. R. Adleman, and D. Psaltis, "Trapping of dielectric particles with light-induced space-charge fields," Appl. Phys. Lett. **90**(24), 241909 (2007).
10. X. Zhang, J. Wang, B. Tang, X. Tan, R. A. Rupp, L. Pan, Y. Kong, Q. Sun, and J. Xu, "Optical trapping and manipulation of metallic micro/nanoparticles via photorefractive crystals," Opt. Express **17**(12), 9981–9988 (2009).
11. M. Esseling, F. Holtmann, M. Woerdemann, and C. Denz, "Two-dimensional dielectrophoretic particle trapping in a hybrid crystal/PDMS-system," Opt. Express **18**(16), 17404–17411 (2010).
12. M. Esseling, A. Zaltron, C. Sada, and C. Denz, "Charge sensor and particle trap based on z-cut lithium niobate," Appl. Phys. Lett. **103**(6), 061115 (2013).
13. J. F. Muñoz-Martínez, I. Elvira, M. Jubera, A. García-Cabañes, J. B. Ramiro, C. Arregui, and M. Carrascosa, "Efficient photo-induced dielectrophoretic particle trapping on $Fe:LiNbO_3$ for arbitrary two dimensional patterning," Opt. Mater. Express **5**(5), 1137–1146 (2015).
14. M. Esseling, *Photorefractive optoelectronic tweezers and their applications* (Springer Theses, 2015).
15. J. F. Muñoz-Martínez, M. Jubera, J. Matarrubia, A. García-Cabañes, F. Agulló-López, and M. Carrascosa, "Diffractive optical devices produced by light-assisted trapping of nanoparticles," Opt. Lett. **41**(2), 432–435 (2016).
16. L. Chen, S. Li, B. Fan, W. Yan, D. Wang, L. Shi, H. Chen, D. Ban, and S. Sun, "Dielectrophoretic behaviours of microdroplet sandwiched between LN substrates," Sci. Rep. **6**(1), 29166 (2016).
17. B. Fan, F. Li, L. Chen, L. Shi, W. Yan, Y. Zhang, S. Li, X. Wang, and H. Chen, "Photovoltaic manipulation of water microdroplets on a hydrophobic $LiNbO_3$ substrate," Phys. Rev. Appl. **7**(6), 064010 (2017).
18. I. Elvira, J. F. Muñoz-Martínez, M. Jubera, A. García-Cabañes, J. L. Bella, P. Haro-González, M. A. Díaz-García, F. Agulló-López, and M. Carrascosa, "Plasmonic enhancement in the fluorescence of organic and biological molecules by photovoltaic tweezing assembly," Adv. Mater. Technol. **2**(8), 1700024 (2017).
19. M. Jubera, I. Elvira, A. García-Cabañes, J. L. Bella, and M. Carrascosa, "Trapping and patternig of biological objects using photovoltaic tweezers," Appl. Phys. Lett. **108**(2), 023703 (2016).
20. S. Grilli and P. Ferraro, "Dielectrophoretic trapping of suspended particles by selective pyroelectric effect in lithium niobate crystals," Appl. Phys. Lett. **92**(23), 232902 (2008).
21. A. Gallego, A. García-Cabañes, M. Carrascosa, and L. Arizmendi, "Pyroelectric trapping and arrangement of nanoparticles in lithium niobate opposite domain structures," J. Phys. Chem. C **120**(1), 731–736 (2016).
22. A. Räuber, "Chemistry and physics of lithium niobate", in *Current Topics in Material Science*, E. Kaldis Ed. (North-Holland Pub. Co., 1978) Chap.7.
23. R. S. Weis and T. K. Gaylord, "Lithium niobate: summary of physical properties and crystal structure," Appl. Phys., A Mater. Sci. Process. **37**(4), 191–203 (1985).
24. S. Grilli, S. Coppola, G. Nasti, V. Vespini, G. Gentile, V. Ambrogi, C. Carfagna, and P. Ferraro, "Hybrid ferroelectric polymer micro fluidic device for dielectrophoretic self-assembling of nanoparticles," RSC Advances **4**(6), 2851–2857 (2014).
25. J. Faba, A. Puerto, J. F. Muñoz-Martínez, A. Méndez, A. Alcazar, A. García-Cabañes, and M. Carrascosa, "Nanoparticle manipulation and trapping by the synergy between the photovoltaic and pyroelectric effects," J. Phys. Conf. Ser. **867**, 012038 (2017).
26. L. Chen, B. Fan, W. Yan, S. Li, L. Shi, and H. Chen, "Photo-assisted splitting of dielectric microdroplets in a LN-based sandwich structure," Opt. Lett. **41**(19), 4558–4561 (2016).
27. A. Savage, "Pyroelectricty and spontaneous polarization in $LiNbO_3$," J. Appl. Phys. **37**(8), 3071–3072 (1966).
28. H. Kurz, E. Krätzig, W. Keune, H. Engelman, U. Gonser, B. Dischler, and A. Räuber, "Photorefractive centers in $LiNbO_3$, studied by optical-methods, moossbauer-methods and EPR-methods," Appl. Phys. **12**(4), 355–368 (1977).
29. F. Johann and E. Soergel, "Quantitative measurement of the surface charge density," Appl. Phys. Lett. **95**(23), 232906 (2009).

Optics EXPRESS

30. I. Nee, M. Müller, K. Buse, and E. Krätzig, "Role of iron in lithium-niobate crystals for dark-storage time of holograms," J. Appl. Phys. **88**(7), 4282–4286 (2000).
31. N. V. Sastry and M. M. Raj, "Densities, speeds of sound, viscosities, dielectric constants, and refractive indices for 1-heptanol + hexane and + heptaneat 303.15 and 313.15 K," J. Chem. Eng. Data **41**(3), 612–618 (1996).
32. J. Matarrubia, A. García-Cabañes, J. L. Plaza, F. Agulló-López, and M. Carrascosa, "Optimization of particle trapping and patterning via photovoltaic tweezers: role of light modulation and particle size," J. Phys. D Appl. Phys. **47**(26), 265101 (2014).
33. L. Lucchetti, K. Kushnir, V. Reshetnyak, F. Ciciulla, A. Zaltron, C. Sada, and F. Simoni, "Light-induced electric field generated by photovoltaic substrates investigated through liquid crystal reorientation," Opt. Mater. **73**, 64–69 (2017).
34. A. Habibpourmoghadam, L. Jiao, V. Reshetnyak, D. R. Evans, and A. Lorenz, "Optical manipulation and defect creation in a liquid crystal on a photoresponsive surface," Phys. Rev. E **96**(2-1), 022701 (2017).
35. A. Habibpourmoghadam, L. Lucchetti, D. R. Evans, V. Y. Reshetnyak, F. Omairat, S. L. Schafforz, and A. Lorenz, "Laser-induced erasable patterns in a N* liquid crystal on an iron doped lithium niobate surface," Opt. Express **25**(21), 26148–26159 (2017).
36. J. Gorecki, V. Apostolopoulos, J. Y. Ou, S. Mailis, and N. Papasimakis, "Optical gating of graphene on photoconductive Fe:$LiNbO_3$," ACS Nano **12**(6), 5940–5945 (2018).